It's All About Statistics: Global Gravity Field Modeling from GOCE and Complementary Data

Roland Pail

Contents

Abstract

Since October 2009, ESA's dedicated satellite gravity mission GOCE (Gravity Field and Steady-State Ocean Circulation Explorer) observes the global gravity field of the Earth. The estimation of the model parameters from the original GOCE observations requires the application of tailored tools of geomathematics and statistics. One of the main constraints is to compute pure GOCE models,

R. Pail (✉)
Institute of Astronomical and Physical Geodesy, TU Munich, Munich, Germany
e-mail: pail@bv.tu-muenchen.de

which are independent of any other external gravity field information. Up to now, four releases of global GOCE gravity field models have been computed and released. Their continuously increasing accuracy is validated by external gravity field information. A key prerequisite for achieving high-quality results is the correct stochastic modeling of all input data types in the frame of a least-squares adjustment procedure based on the rigorous solution of full normal equation systems. Together with the global gravity field models, parameterized as coefficients of a spherical harmonic series expansion, also the related error variance-covariance matrix is generated, which turns out to describe the true errors of the solutions very accurately. The fourth release achieves global geoid height accuracies of 3.5 cm and gravity anomaly accuracies below 1 mGal at a spatial wavelength of 100 km. Further improvements are expected, also because of the GOCE satellite's orbit lowering in its final mission phase, which will further improve the spatial resolution. In addition to these pure GOCE-only models, in the frame of the GOCO initiative consistent combined gravity field models are processed by including GRACE and SLR data (improving the long wavelengths), as well as terrestrial gravity information and satellite altimetry (improving the high-frequency component). Also for the computation of these optimum combinations, the tools developed for the GOCE processing can largely be applied. Numerous fields of application in geodesy, oceanography, and geophysics can benefit already now from the new GOCE models. As an example, the derivation of global ocean transport processes from a combination of satellite altimetry and global gravity information demonstrates that GOCE can contribute significantly to an improved understanding of processes in system Earth.

1   Introduction

The gravity satellite mission GOCE (Gravity Field and Steady-State Ocean Circulation Explorer), the first Earth Explorer Core Mission in the frame of the Living Planet Programme executed by the European Space Agency (ESA), was successfully launched on March 17, 2009 into a very low orbit of only about 255 km altitude. Since October 2009, the mission has been in science mode and is continuously delivering operational data. The main goal of GOCE is the determination of the Earth's static gravity field with unprecedented accuracy and spatial resolution, with a specification of 2 cm geoid height and 1 mGal gravity anomaly performance at a spatial wavelength of 100 km (Floberghagen et al. 2011).

The measurement concept of GOCE is based on sensor fusion: The long wavelength component of the global Earth's gravity field is derived from high-precision orbit information of the satellite. In this case, the satellite as a whole is used as a test mass flying in the irregular gravity field of the Earth, leading to orbit perturbations. The orbit is determined with a 3D standard deviation of only

2–3 cm (Bock et al. 2011) by GPS positioning applying satellite-to-satellite tracking in high-low mode (hl-SST) between the GPS satellites and the low Earth orbiter GOCE. The medium to short wavelengths down to 80 km are measured by the core instrument of GOCE, the so-called gravity gradiometer, a payload which has been manufactured and flown for the very first time ever. Its measurement principle, satellite gravity gradiometry (SGG), is based on the observation of second-order derivatives of the Earth's gravitational potential This is realized by 6 accelerometers fixed on 3 orthogonal axes symmetrically around the center of mass of the satellite, measuring acceleration differences on very short baselines of only half a meter in all 3 dimensions ("differential mode"). Apart from that, the gradiometer also measures the nonconservative forces, such as the air drag, solar radiation pressure, or thruster events, as a mean value of two accelerometer readings along one axis ("common mode"). These nonconservative accelerations are actively compensated in real time by the drag-free and attitude control system (DFAC) and ion thrusters, thus keeping the satellite virtually in free fall in the gravity field of the Earth. Only this permanent drag compensation allows keeping the satellite on a constant low altitude of only 255 km for the whole mission period of more than 3 years, enabling gravity field observations close to the Earth and thus achieving a high spatial resolution of the detail structures of the gravity field. A detailed discussion of the GOCE measurement principle and the mission setup can be found in Rummel (2010). In Freeden and Schreiner (2010), SGG is interpreted and discussed as spacewise inverse problem.

The computation of models of the global gravity field from GOCE orbit (hl-SST) and gradiometry (SGG) data, and on a later stage also including complementary satellite and terrestrial gravity field data, is a demanding task. A whole arsenal of methods of geomathematics, statistics, and numerics, forming tailored processing algorithms and procedures, have to be applied to achieve optimum solutions (in least-squares sense). In this contribution, an overview of the statistical toolkit for the modeling of the global gravity field shall be presented and discussed on the example of the GOCE mission. More generally, it can also serve as a case study and recipe for the estimation of large parameter models from a very large number of observations with arbitrary noise characteristics.

Correspondingly, in Sect. 2, the global gravity field of the Earth and its parameterization is described, from which the functional and stochastic models are derived. Section 3 presents the processing chain, being composed of a toolkit of statistical and numerical methods. In Sect. 4, the application of these algorithms to real GOCE data and the resulting global gravity field models are presented. In Sect. 5, current and future perspectives of the GOCE mission are outlined, such as combined gravity field modeling by including complementary gravity data, the gain of accuracy due to improvements in the Level 1b preprocessing methodology, and the satellite's orbit lowering in its final mission phase. Finally, in Sect. 6, the main results are summarized, and the impact of the new GOCE models in different fields of application is discussed.

2   The Global Gravity Field: Functional Model

The global Earth's gravitational potential V is usually parameterized by a spherical harmonic series expansion, which results from the solution of Laplace equation $\Delta V = 0$ in spherical coordinates (radius r, co-latitude ϑ, and longitude λ):

$$V(r, \vartheta, \lambda) = \frac{GM}{R} \sum_{n=0}^{L} \left(\frac{R}{r}\right)^{n+1} \sum_{m=0}^{n} \bar{P}_{nm}(\cos\vartheta)[\bar{C}_{nm}\cos(m\lambda) + \bar{S}_{nm}\sin(m\lambda)]$$

$$= \sum_{n=0}^{L} \sum_{m=0}^{n} A_{nm} x_{nm} \tag{1}$$

where G is the gravitational constant; M and R are the Earth's mass and reference radius, respectively; $\bar{P}_{nm}$ the fully normalized Legendre polynomials of degree n and order m; and $x_{nm} = \{\bar{C}_{nm}; \bar{S}_{nm}\}$ the corresponding coefficients. Main goal of global gravity field modeling is to determine the coefficients of the series expansion $\{\bar{C}_{nm}; \bar{S}_{nm}\}$ as well as corresponding error information up to a certain maximum degree of the series expansion L (in theory, the maximum degree in Eq. (1) is $L = \infty$) in an "optimum" way from the gravity field observations, which are functionals of the gravitational potential V. Equation (1) represents the basic functional model and observation equation in the frame of the gravity field solution.

A more precise approximation of the geometrical Earth's figure is the expansion in ellipsoidal harmonics (e.g., Grafarend et al. 2010), which is, however, much more costly from a computational point of view and, therefore, will not be further considered in this study.

In the case of GOCE, the observations are – apart from kinematic GPS orbit obtained by precise orbit determination (Bock et al. 2011) – the gravitational gradients, forming second-order spatial derivatives of the gravitational potential

$$V_{ij} = \frac{\partial^2 V}{\partial x_i \partial x_j} \tag{2}$$

in a local rotating reference frame, whose axes x_i, with $x_i = X, Y, Z$, are oriented along the gradiometer axes (Gradiometer Reference Frame; GRF). The GRF deviates from an ideal, radially oriented local orbit reference frame by 3˚–5˚ (Rummel et al. 2011).

They form a 3×3 matrix (the so-called Marussi tensor), which is symmetric $\left(\text{because of } \frac{\partial^2}{\partial x_i \partial x_j} = \frac{\partial^2}{\partial x_j \partial x_i}\right)$ and has only five independent elements, due the Laplace equation $\Delta V = V_{XX} + V_{YY} + V_{ZZ} = 0$ forming a condition for the tensor's trace.

As any measurement device, also the six accelerometers composing the gradiometer are affected by noise with specific spectral characteristics. Figure 1 shows the spectral behavior of the gradiometer noise in terms of a power spectral density
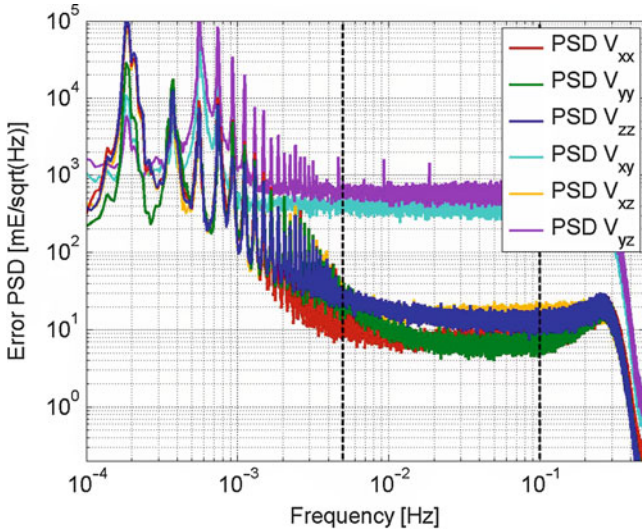
Fig. 1 Noise PSD of the 6 GOCE gravity gradient components

for all six gradiometer components V_{ij}. The lower performance of the two off-diagonal components V_{XY} and V_{YZ} by a factor of 100 results from the fact that each of the six individual accelerometers has two high-sensitive and one less-sensitive axes. The specific mounting within the gradiometer leads to the fact that the three in-line components V_{XX}, V_{YY}, V_{ZZ}, holding the main gravity field information, and V_{XZ}, which is especially sensitive to the main satellite's rotational motion, have the highest performance. As it will be discussed in Sect. 3.4, it is of utmost importance to include this information on the actual gradiometer noise characteristics as stochastic model in the solution strategy.

3   GOCE Gravity Field Modeling

Figure 2 shows the architectural design of global gravity field processing, which is composed of a multitude of methods and problems of geomathematics and statistics, such as statistical methods for outlier detection, stochastic modeling via recursive digital filters, optimum relative weighting of different data types and groups, regularization to stabilize the solution, parameter estimation by least-squares adjustment, and covariance propagation, to finally end up with an "optimum" gravity field solution plus corresponding variance-covariance information.

Here we follow the processing approach of the so-called time-wise method (TIM; Pail et al. 2010a) to derive TIM gravity field models as a joint effort of TU München, Graz University of Technology, and University of Bonn. This is part of the ESA project "High-Level Processing Facility" (Rummel et al. 2004),
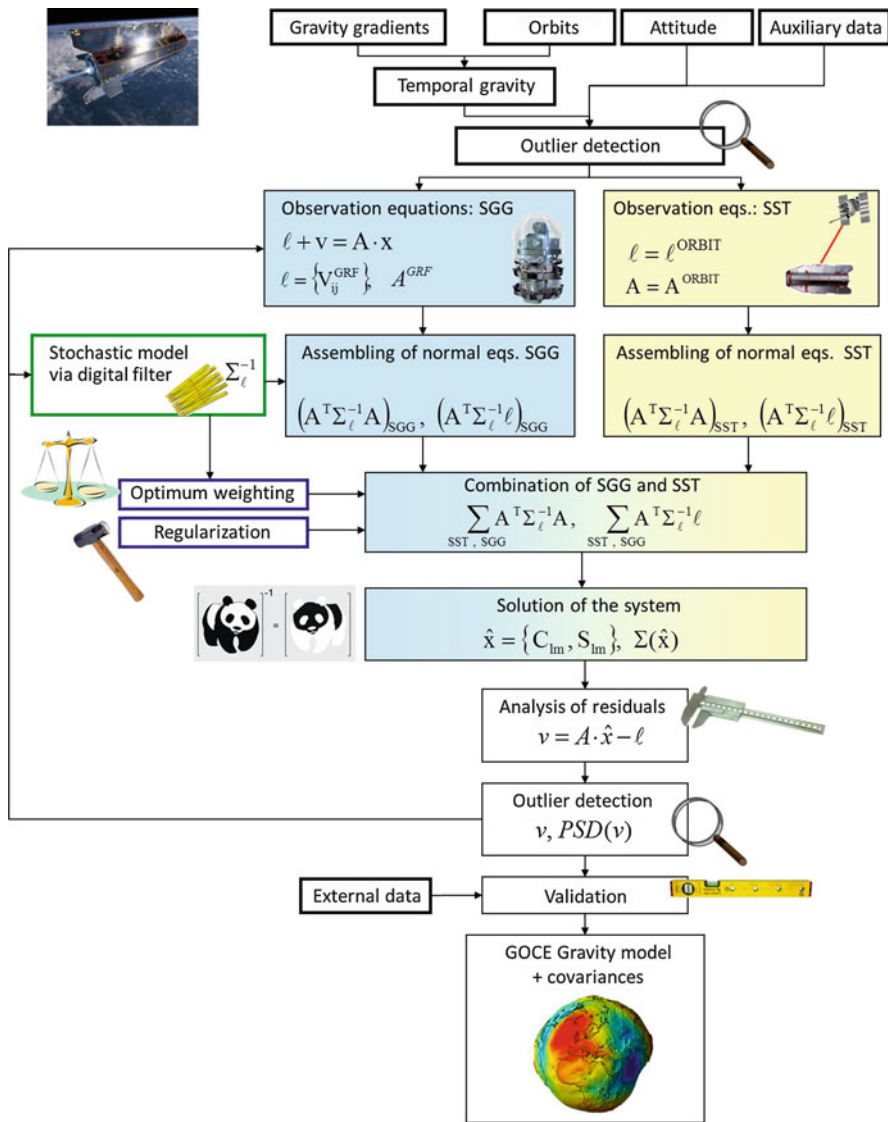
Fig. 2 Architectural design and key processing steps of GOCE gravity field modeling

a consortium of 10 European universities and research institutions, managed by TU München. Apart from the TIM models, two other processing strategies are applied within HPF: the "direct method" (DIR; Bruinsma et al. 2010) and the "spacewise method" (SPW; Migliaccio et al. 2010). While TIM and DIR are based on a least-squares adjustment approach applied to observations sequentially along the orbit,

SPW considers the regional spatial distribution of the observation and applies a least-squares collocation approach (Moritz 1978).

It is a specific feature of the gravity field modeling method described here that it produces GOCE-only model in a rigorous sense, i.e., no external gravity field information is used, neither as reference model nor for constraining the solution. Correspondingly, the resulting gravity field solutions are based solely on GOCE data and are independent of any complementary gravity field information.

3.1   Input Data

Key input products to be used for gravity field modeling (product identifiers according to EGG-C (2010)) comprise:

- Precise Science Orbits: SST_PSO_2I, including the subproducts:
    - SST_PKI_2I: kinematic orbits
    - SST_PCV_2I: variance-covariance information of orbit positions
    - SST_PRD_2I: reduced-dynamic orbits
    - SST_PRM_2I: quaternions for transformation from Earth-fixed to inertial reference frame
- Gravity Gradients in the GRF: EGG_NOM_2
- Attitude Quaternions: EGG_IAQ_2C (corresponds to columns 56–59 of EGG_NOM_2)

The main objective is to derive a static GOCE gravity field. Therefore, time-variable signals have to be reduced a priori from the orbit (SST) and gravity gradient (SGG) measurement time series. Correspondingly, models for temporal gravity field reduction, such as ephemerides of Sun and Moon (AUX_EPH), ocean tide models (ANC_TIDE, ANC_TID_2I), correction coefficients for non-tidal temporal variation signals (SST_AUX_2I), and for Earth rotation (AUX_IERS), have to be applied.

Additionally, for the processing of gravity fields from orbits, nongravitational accelerations, as they are measured by the gradiometer in common mode and given in the product EGG_CCD_2C, are applied.

3.2   Data Preprocessing

The reduction of temporal gravity field signals is mainly important for the SST observations, since they are sensitive to long-wavelength signals which contain the largest temporal gravity field signals, while due to the error characteristics of the gravity gradients as shown in Fig. 1, temporal gravity is usually not visible. However, it should be emphasized that many temporal gravity field signals show periodic behavior, such as semidiurnal and diurnal ocean tides. They comprise a

systematic signal and thus are not fully reduced by averaging and, therefore, play a more and more significant role the longer the GOCE mission continues.

Outlier detection is applied using an arsenal of statistical methods (Kern et al. 2005) in order to identify at least coarse outliers, resulting in outlier flag files indicating those epochs which shall not be assembled. However, the fine-tuned outlier detection can only be done based on the residuals of a previous gravity field adjustment, because smaller outliers can only be detected on the residual level, but not on the level of the full signals. Therefore, usually a feedback loop is applied (cf. Fig. 2) to recompute the gravity field model after outlier detection on the basis of residuals with an updated outlier flag file and potentially also an updated stochastic model (cf. Sect. 3.4).

Another preprocessing step is the synchronization of the gravity gradient and orbit time series, where the orbits are interpolated to the SGG epochs applying a Newton interpolation scheme (Goiginger and Pail 2007).

3.3   Observation Equations

SGG and SST normal equations (NEQs) are set up separately, where the SST NEQs are resolved to maximum degrees of 100–150.

The information content of the SST data is exploited by making use of the precise GOCE orbit expressed in terms of position information including quality description. Kinematic orbits (SST_PKI) are purely geometrical orbit solutions solely based on the GPS observations, without including any gravitational and nongravitational force models. Although the noise level, which is in the order of 2–3 cm 3D rms (Bock et al. 2011), is higher than for reduced dynamic orbits (SST_PRD), only when using kinematic orbits it is guaranteed that external gravity field information is not introduced via the backdoor. For the TIM releases 1–3, the principle of energy conservation has been applied in an inertial reference frame (Badura 2006) to derive the gravity field from kinematic orbits. Starting from TIM release 4, the short-arc method (Mayer-Gürr et al. 2010) is applied. In the energy conservation method, pseudo-observations in terms of the (scalar) kinetic energy are computed from the orbit velocities, which have been previously derived from the kinematic orbit positions by numerical differentiation (Goiginger and Pail 2007). In contrast, the short-arc method fully exploits the 3D orbit information and thus outperforms the energy integral method by a factor of about $\sqrt{3}$. The use of the covariance information (SST_PCV) as stochastic model for the SST observations shows some advantages especially concerning the correct error description of the resulting gravity field coefficients (Goiginger and Pail 2010). Details on the SST processing can be found in Pail et al. (2010a, 2011). In the following, we will mainly concentrate on the SGG component.

The observation equations of the SGG for the following least squares adjustment based on a standard Gauss-Markov model can be derived by combining Eqs. (1) and (2):

$$\ell_{SGG} + v = V_{ij}^{GRF} + v = \sum_{n=0}^{L} \sum_{m=0}^{n} (A_{ij}^{GRF})_{nm} x_{nm} = A_{SGG} x \qquad (3)$$

Since the measurement accuracy of the off-diagonal gradient tensor components V_{XY} and V_{YZ} is worse by a factor of about 100, only the other four gravity gradient components (main diagonal components V_{XX}, V_{YY}, V_{ZZ} and off-diagonal component V_{XZ}) are used for gravity field modeling. In order to avoid rotation of the observed gravity gradients V_{ij}^{GRF} to an ideal Earth-fixed frame, whereby the high-accuracy gravity gradient components would suffer from a severe deterioration due to an aliasing of the low-accuracy off-diagonal gradient tensor components V_{XY} and V_{YZ}, instead the base functions $(A_{ij}^{GRF})_{nm}$ are rotated to the GRF before assembling.

The detail procedure is the following: first, the spherical harmonic base functions for all gravity gradient tensor components are computed in an ideal radial and north-oriented Earth-fixed reference frame at the satellite's position, which has been interpolated from the orbit products for the observation epoch of the gradients. Then the base functions are rotated to the GRF. The rotation matrix is composed of two pieces of information: the rotation matrix from the Earth-fixed to the inertial frame (part of the orbit product SST_PRM, interpolated consistently to the SGG epochs) and the attitude quaternions providing the rotation from the inertial frame to the GRF. The combined rotation matrix is then applied to all base function elements, yielding $(A_{ij}^{GRF})_{nm}$. Finally, only the four selected tensor elements related to the high-accuracy gravity gradients ($ij = XX, YY, ZZ$ or XZ) are used for assembling the SGG NEQs.

3.4 Stochastic Modeling

Due to the colored noise characteristics of the gradiometer observations (cf. Fig. 1), the correct stochastic modeling of the observation errors is a key requirement to obtain high-quality gravity field solutions. The decreased performance of the gradiometer in the low-frequency range results in long-wavelength correlations of the SGG observation noise. In order to demonstrate this effect very lucidly, Fig. 3 (left column) shows typical amplitudes of the signal (top), the gradiometer noise (middle), and the actual observations (bottom) containing signal and noise, of the radial component V_{ZZ} at mean satellite altitude, projected to a regional grid. Evidently, the signal is superimposed with predominantly long-wavelength error structures, demonstrating the need for an optimum signal-noise separation as main task of the gravity field adjustment.

Assuming the observation errors to be a stochastic process, causal digital recursive filters of ARMA type (Auto-Regressive Moving Average) are used to approximate the error behavior of the observations (Klees et al. 2003; Schuh 1996; Siemes 2008) and thus to comprise the stochastic model Σ_ℓ, which shall introduce the actual error information of the gravity gradient observations as weight matrix
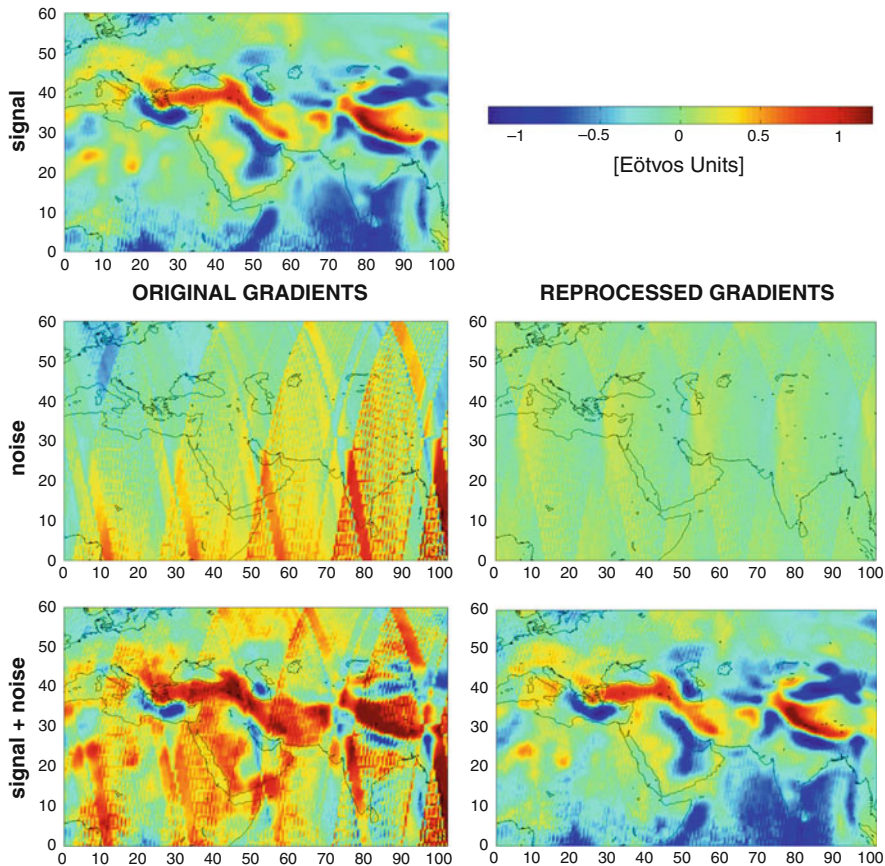
Fig. 3 V_{ZZ} gradients [E] in mean orbit altitude projected on a regional grid; *top*, signal (degree/order 200); *middle*, noise; *bottom*, signal + noise; *left column*, original gradients (cf. Sect. 3.4); *right column*, reprocessed gradients (cf. Sect. 5.2)

and thus as the metric into the NEQs. The basic idea shall be sketched in the following.

Since the stochastic part of the observations ℓ is affected by colored noise, we design a filter F which shall ideally produce, when applied to the colored noise time series, uncorrelated, normal-distributed random noise with mean $\mu = 0$ and variance $\sigma^2 = 1$. Applying this (lower triangular) filter matrix F to the observation vector ℓ and the columns of the design matrix A_{SGG} (in the following abbreviated by A for the sake of simplicity)

$$\bar{\ell} = F\ell, \tag{4a}$$

$$\bar{A} = FA, \tag{4b}$$

the unbiased L2 solution of this Gauss-Markov system is obtained by

$$\hat{x} = (\bar{A}^T \bar{A})^{-1} \bar{A}^T \bar{\ell} = (\bar{A}^T I \bar{A})^{-1} \bar{A}^T I \bar{\ell}, \tag{5}$$

where the unit matrix I indicates that ideally the projected (filtered) system should be fully decorrelated and obeys $N(\mu = 0, \sigma^2 = 1)$.

Inserting for the filtered quantities Eqs. (4a) and (4b) into Eq. (5) yields

$$\hat{x} = (A^T F^T FA)^{-1} A^T F^T F\ell. \tag{6}$$

Comparing Eq. (6) with the solution of a general unbiased Gauss-Markov model $N(0, \Sigma_\ell)$,

$$\hat{x} = (A^T \Sigma_\ell^{-1} A)^{-1} A^T \sum_\ell^{-1} \ell \tag{7}$$

reveals that the inverse variance-covariance matrix of the observations Σ_ℓ can be expressed by the filter matrix as

$$\Sigma_\ell^{-1} = F^T F. \tag{8}$$

A computationally efficient way to introduce the stochastic model into the NEQs is to formulate the filter operation as a digital recursive filter, $F = F(a_k, b_k)$, in time domain, applied to the observation equations. Here we are using causal digital ARMA filters, which are described by filter coefficients (a_k, b_k) defining the poles (AR part) and zeros (MA part) of the filter, respectively, and thus the weights of the linear combination of elements of the input series y_{s-k} and the filtered output series $\bar{y}_{s-k}$ at the current epoch s:

$$\bar{y}_s = \sum_{k=0}^{N_b} b_k y_{s-k} - \sum_{k=1}^{n_a} a_k \bar{y}_{s-k}. \tag{9}$$

Technically, this is done by applying these filters to the full observation equation, i.e., y_s stands for both, the observation vector ℓ and the columns of the design matrix A, leading ideally to a full decorrelation (whitening) of the time series. In this way, the gradiometer error information is introduced as the metrics of the NEQ system, thus describing the weighting of the observations. It shall be emphasized that when designing the filters, only the amplitude spectrum has to be considered. Since the normal equations are of quadratic nature, the phase becomes automatically zero when the filter operator is squared (multiplied by its conjugate complex), as it is done in the composition of $A^T F^T FA$ and $A^T F^T F\ell$.

As an example, the red curve in Fig. 4 shows an ARMA filter model (magenta) for the gradient component V_{ZZ}, approximated to the estimate of the gradiometer noise derived from the residuals of a previous gravity field adjustment (cf. Sect. 3.6). In order to fit the actual error characteristics more easily, filter cascades composed
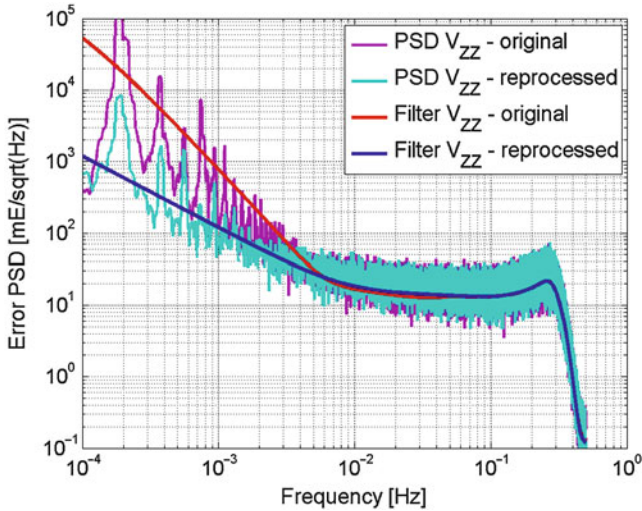
Fig. 4 Noise PSDs and approximated filters of gravity gradient component V_{ZZ} for original (cf. Sect. 2) and reprocessed (cf. Sect. 5.2) gravity gradients

of two (or more) individual filters of different complexity, which are applied sequentially, can be designed: $F = \prod_{i=1}^{k} F_i$.

Usually, filter orders N_a, N_b of 10–50 are sufficient to approximate the gradient error behavior properly. Special attention has been given to the fact that the designed filters have a relatively low filter order and thus are computationally efficient. Applied in time domain and starting with no information from the past, the filters require a certain period until they work correctly. Therefore, an important aspect is to design filters that have short warm-up times of only a few hundred to thousand epochs, which are only used to run the filters, but are not assembled (Stetter 2012). Therefore, also data gaps and outlier-flagged epochs pose a problem and require special treatment in order to minimize the data loss (Siemes 2008).

In summary, it shall be emphasized that with this stochastic modeling procedure, we do not filter out certain spectral components of the gradients, but we try to give them their proper weight in the course of the gravity field adjustment.

3.5 Excursion: The Role of the Measurement Bandwidth

In Sect. 2, it has been shown that the gradiometer performs best within the MBW of 5–100 MHz, where it is approximately white, while below it degrades significantly toward low frequencies, with 1/frequency characteristics. One of the simplest

but also questionable approaches to get rid of this colored noise behavior is by filtering the gradients to the measurement bandwidth. In this subsection, it shall be demonstrated that this is a highly unfavorable approach. Due to the fact that there is no one-to-one correspondence between the frequency spectrum of the gravity gradient time series and the spherical harmonic spectrum of the gravity field, band-pass filtering represents a highly anisotropic filter in spatial domain, i.e., the filtered signal will contain completely different spectral signal content in north-south and east-west direction.

The danger of such an approach becomes evident when such a filtered signal is then used as the basis for geophysical interpretation. However, the effect of such an approach can also nicely been shown in the frame of gravity field modeling. For this purpose, a simplified, simulated test configuration was set up, where the "true" gravity field signal in terms of gravity gradients V_{XX}, V_{YY}, and V_{ZZ} was synthetized from a known gravity field model complete to degree/order 200. In two test runs, different noise time series were superimposed, and the gravity field was recovered and compared with the "true" input model. While in the first configuration, realistic noise as shown in Fig. 1 was assumed (blue curve in Fig. 5, top), in the second test run, a high error level with an amplitude, which is by a factor of 100 higher than in the MBW, was assumed for all frequencies below and above the MBW (red dashed curve in Fig. 5, top). This high noise level shall mimic the fact that we have no (or in our case only very bad) information of the gravity field signal below the MBW.

The middle row of Fig. 5 shows the mapping of these gradiometer errors to SGG-only gravity field solutions. In the first configuration (right), almost all coefficients, except of the very low degrees and the (near)zonal ones (due to the polar gap problem; cf. Sect. 3.6), can be estimated reasonably well. In contrast, if only the information within the MBW is considered (left), in addition, mainly the sectorial and near-sectorial coefficients up to degree/order 120 are retrieved with significantly reduced accuracy. This proves that the spectral range below the MBW contains important information for the estimation of coefficients of rather high degree. Additionally, it shall be emphasized that cutting off the signal at the MBW acts as an extremely anisotropic filter. This is reflected by the fact that coefficients of a certain degree (and thus corresponding to a certain spatial wavelength) are retrieved with very different accuracy. An even more obvious picture of this anisotropic behavior is provided at the bottom row of Fig. 5, where the corresponding errors in terms of gravity anomaly deviations from the true reference model up to degree/order 200 are displayed. The weakness of the (near-)sectorial coefficients in the left case is reflected by the North-South striping structures.

In summary, it can be concluded that the information below the MBW is essential to process GOCE-only models. The missing gravity field information when filtering the gravity gradients cannot be fully compensated by an addition of the hl-SST component, due to the fact that coefficients even up to degree/order 120 are affected. Equally important, it is dangerous to use band-pass filtered gradients for geophysical interpretation!
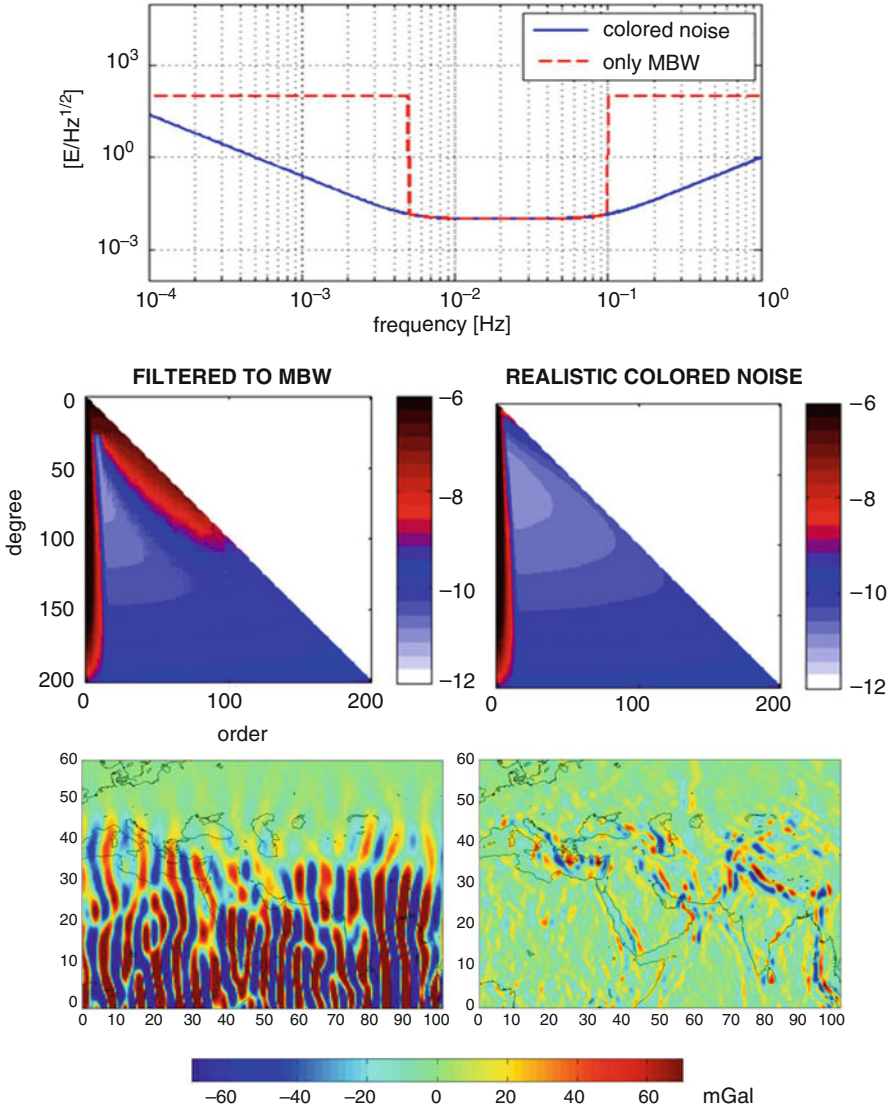
Fig. 5 Analysis of effect of band-pass filtering of gradients. *Top*, gravity gradient noise spectra (exemplarily for V_{ZZ}); *middle*, mapping to SH coefficients; *bottom*, gravity anomaly error [mGal]s. *Left column*, gravity gradients filtered to MBW; *right column*, full spectral range used

3.6   Normal Equation Setup and Solution

Full normal equation for hl-SST and SGG is assembled separately (cf. Fig. 2). For a gravity field model up to degree/order 250, about 63,000 parameters and the corresponding error information in the form of a full variance-covariance matrix

are solved rigorously on a Linux cluster system, applying least-squares adjustment based on a standard Gauss-Markov model. The complete normal equations read

$$(w_{SGG} N_{SGG} + w_{SST} N_{SST} + \alpha N_{CAP})\hat{x} = w_{SGG} n_{SGG} + w_{SST} n_{SST} + \alpha n_{CAP}, \tag{10}$$

where N stands for the normal equation matrix of a specific component, $N = A^T \Sigma_\ell^{-1} A$, and n for the right-hand side, $n = A^T \Sigma_\ell^{-1} \ell$.

For gravity gradiometry, usually the three main diagonal components V_{XX}, V_{YY}, V_{ZZ} and the high-precision off-diagonal component V_{XZ}, defined in the GRF, are used. However, it can be shown that the high-accuracy off-diagonal gravity gradient component V_{XZ} (cf. Fig. 1) adds only marginal contributions to the solution, due to its sensitivity to attitude errors (Pail 2005).

Optimum relative weights w of the individual components are estimated applying variance component estimation (Koch and Kusche 2002). Due to the fact that as realistic as possible stochastic models Σ_ℓ are used as metric of the NEQ (cf. Sect. 3.4), the resulting relative weights usually are close to "1."

Specific attention has to be given to constraining the combined NEQ system, which is usually ill-conditioned mainly due to the so-called polar gap problem. Since the satellite flies a sun-synchronous orbit with an orbit inclination of $i = 96.6°$, the polar areas are not covered with measurements, leading to a very inhomogeneous data distribution. It can be shown that the polar gap has a much higher impact on the ill-conditioning than the downward continuation, by 2–3 magnitudes. To counteract this problem, the spherical cap regularization approach (Metzler and Pail 2005) was developed. Here, spherical polar caps are defined as additional normal equations N_{CAP}, playing the role of the regularization matrix. The corresponding right-hand side n_{CAP} can either be filled by zeros (corresponding to a constraint toward a zero model) or by an analytical function which is only defined in the cap region. It can be shown that with a reasonable choice of the regularization parameter α, the impact of this regularization remains restricted to the polar caps, while the regularization bias is negligible in those areas which are covered with measurements. An easy alternative is to apply a classical Kaula regularization only to those coefficients which are affected by the polar gap, according to the rule of thumb given by Sneeuw and van Gelderen (1997).

In order to improve the signal-to-noise ratio in the very high degrees, additionally Kaula regularization is usually applied for all coefficients above a certain degree (170 for TIM release 1, 180 for releases 2–4). The optimum regularization parameter α is determined jointly with the optimum weights w in the frame of the abovementioned variance component estimation.

Finally, after combination of all components and their optimum weighting, the coefficient solution is computed by a parallel Cholesky decomposition scheme (Pail and Plank 2002), and the corresponding full variance-covariance matrix is obtained by explicit inversion of the NEQs.

3.7 Analysis of Residuals

The analysis of the residuals of the gravity field adjustment, i.e., the differences between the original observations and those computed from the estimated gravity field coefficients, is a valuable tool to get an idea of the instrument performance, especially concerning the individual gravity gradient components. In the first approximation, the power spectral density of the gravity gradient residuals provides the noise characteristics of the SGG observations and thus of the gradiometer transition function.

The idea behind this strategy can be outlined as follows: the observation equations (Eq. 3) can be reformulated using the unknown parameter vector x and the unknown true errors ε:

$$\ell - \varepsilon = A \, x. \tag{11}$$

Unbiasedness $E\{\hat{x}\} = x$ provided, the residuals v can be considered as estimates for the (negative) true errors $-\varepsilon$. A transformation of ε into the frequency domain $PSD\{\varepsilon\}$ (corresponding to a (squared) discrete Fourier transform $F\{\varepsilon\}$ which is normalized by a time unit to obtain a spectral density) corresponds to the (true) gradiometer error PSD. Therefore, the spectral analysis of the residuals $PSD\{v\}$ should approximate the gradiometer transition function,

$$PSD\{v\} \approx PSD\{\varepsilon\}, \tag{12}$$

but only if the system is consistent, i.e., in the absence of any systematic errors in the observations.

The main assumption here is that the sum of all errors projected into the SGG residuals are dominated by the gradiometer errors themselves, while other errors resulting from attitude reconstruction and non-precise geolocation due to orbit errors play a minor role. It can be shown that this assumption is largely true, with the exception of the very low frequencies, where the attitude errors dominate the total error budget (Pail 2005). For the purpose of geolocation, orbit accuracies of 2–3 m would be sufficient. (It should also be emphasized that in the gravity field adjustment from SGG, only the gravity gradients are assumed as stochastic quantities, while attitude and orbit are assumed to be known deterministic.)

The gravity gradient residuals are the basis for the stochastic modeling as described in Sect. 3.4.

3.8 Data Inspection

The correct working of the filters derived in Sect. 3.4 can be proved a posteriori by applying them to the post-fit residuals of the gravity field adjustment, because

ideally this operation should lead to a normal distributed white noise time series with variance $\sigma^2 = 1$. This can be tested applying appropriate hypothesis tests (Kargoll 2007; Lackner 2006).

As already mentioned in Sect. 3.2, also the main outlier detection is performed in the frame of gravity field processing based on the gravity gradient residuals, because they have a much smaller amplitude than the full signal, so that outliers become more distinct.

3.9   Validation

There are different methods to validate the resulting GOCE gravity field models. Due to the fact that they represent models with unprecedented accuracy and spatial resolution, their validation is not an easy task.

A straightforward and commonly used strategy is to compare the new GOCE models with existing global gravity field models of the pre-GOCE era in regions where these models are known to be good. Additionally, GOCE results can be compared in regions with high-quality terrestrial gravity data and with "directly measured" geoid heights derived from a combination of long-term GPS observations and spirit leveling. Over the oceans, the geodetic mean dynamic topography (MDT) can be computed as the difference of the geometric sea surface derived from satellite altimetry, and the geoid computed from the global model to be validated. The resulting MDT can then be compared with independently computed MDT estimates, either derived from ocean models or in situ drifter measurements. The long-wavelength part can be validated in the frame of orbit tests, by using the gravity field model in a dynamic orbit solution for low-orbiting satellites and comparing the integrated orbit with actual GPS observations. An overview of different validation methods and their application to GOCE gravity fields can be found in Gruber et al. (2011).

4   Results

In the following, the main results of the releases 1–4 of TIM gravity field models are discussed, and their performance is assessed and validated. Table 1 summarizes the main characteristics of these models, such as the maximum degree of resolution, the gradient data type, the data period, as well as the net number of epochs contained in the solutions. The last two columns provide their accuracy in terms of global geoid height and gravity anomaly errors at 100 km spatial resolution ($L = 200$).

Figure 6 shows the achieved performance in terms of the degree medians of the formal errors:

$$\sigma_n = median_m\{\sigma_{\bar{C}_{nm}}, \sigma_{\bar{S}_{nm}}\} \tag{13}$$

Table 1 Main characteristics of TIM gravity field models

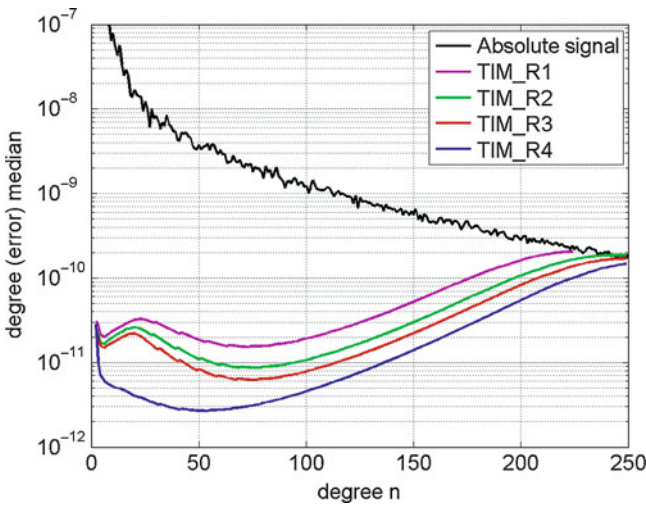| Model	Max. degree	Gradients	Data period	# epochs (in mio.)	σ_N [cm] (d/o 200)	$\sigma_{\Delta g}$[mGal] (d/o 200)
TIM_R1	224	Original	01/11/2009–11/01/2010	6.2	10.0	3.0
TIM_R2	250	Original	01/11/2009–05/07/2010	19.5	6.1	1.8
TIM_R3	250	Original	01/11/2009–17/04/2011	31.3	4.6	1.3
TIM_R4	250	Reprocessed	01/11/2009–19/06/2012	69.7	3.2	0.9

Fig. 6 Degree error medians of the GOCE-only TIM gravity field solutions

It illustrates the continuous improvement of the achieved accuracy by including more and more GOCE data. The gains follow the Gaussian covariance propagation law of uncorrelated observations of $\sqrt{N}$. Correspondingly, the improvement from TIM_R1 to TIM_R2, which contains approximately the threefold data volume, is about $\sqrt{3}$; TIM_R3 improves with respect to TIM_R2 by a factor of almost $\sqrt{2}$ and TIM_R4 with respect to TIM_R3 again by a factor of $\sqrt{2}$. The significantly improved performance of release 4 in the low degrees results from the switching from the energy integral to the short-arc method concerning the hl-SST processing (cf. Sect. 3.3), and additional improvements over the whole spectral range result from the use of reprocessed gravity gradient products (cf. Sect. 5.2).

Several external validations show that due to the realistic stochastic modeling of all observation components (SGG components, hl-SST), the formal errors reflect quite realistically the true accuracies of the TIM gravity models. Figure 7 shows the global distribution of geoid height accuracies at degree/order 200, resulting
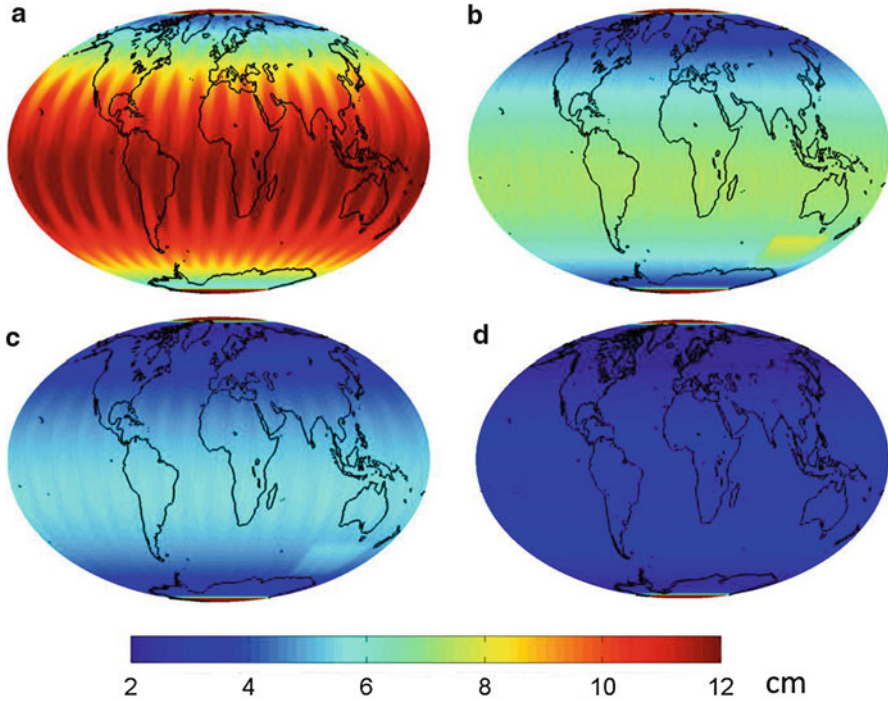
Fig. 7 Geoid height standard deviations at degree/order 200 derived by covariance propagation from the full VCM: (**a**) TIM_R1; (**b**) TIM_R2; (**c**) TIM_R3; (**d**) TIM_R4

from a rigorous covariance propagation of the parameter variance-covariance matrix (VCM) $\Sigma(\hat{x})$ to geoid heights. The asymmetry with respect to the equator results from the specific GOCE orbit configuration, i.e., a slightly larger average orbit altitude in the Southern Hemisphere. The characteristic structure south of Australia in TIM_R2 and TIM_R3 reflects data problems of the V_{YY} component. These erroneous gradient observations have been eliminated regionally, leading to a smaller number of observations in these regions. This proves that the VCM nicely reflects specific data anomalies and their impact on the solution.

The estimated cumulative geoid height and gravity anomaly accuracies at degree/order 200 of the four TIM releases are summarized in Table 1.

The analysis of the formal errors is only one side of the medal to assess the real accuracy of a gravity model. Therefore, the results have also been compared with the independent global gravity model EGM2008 (Pavlis et al. 2012), which contains mainly GRACE data, terrestrial gravity, and satellite altimetry data over the oceans.

Figure 8 shows gravity anomaly differences to EGM2008 up to degree/order $L = 200$ for the regions of North America (top) and South America (bottom). The left column provides difference fields of TIM_R1 and the right column of TIM_R4. Table 2 summarizes the corresponding standard deviations, computed in
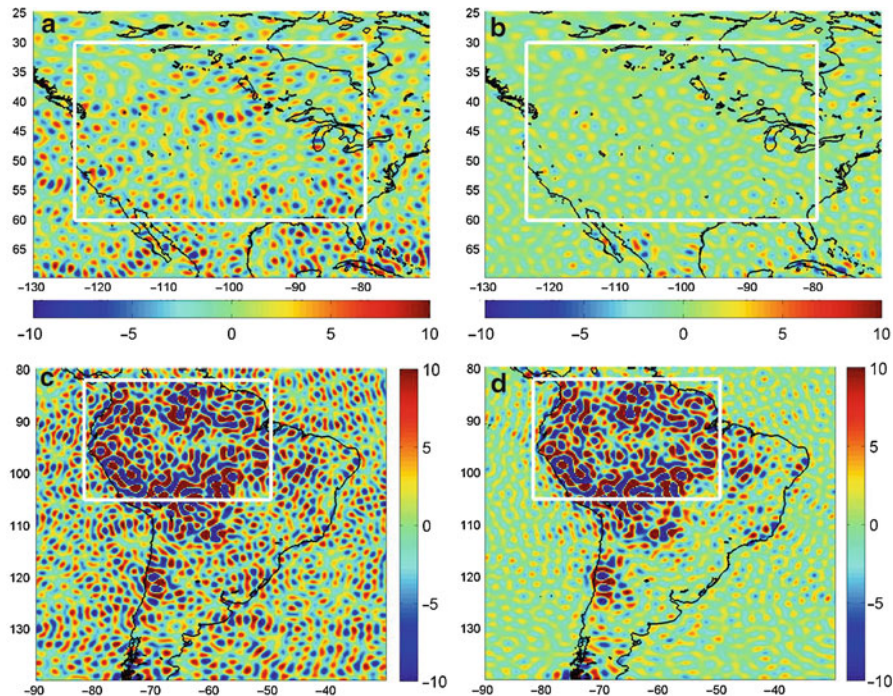
Fig. 8 Gravity anomaly differences [mGal] to EGM2008 in North America (*top row*) and South America (*bottom row*), for TIM_R1 (*left column*) and TIM_R4 (*right column*)

Table 2 Standard deviations of gravity anomaly differences of different GOCE TIM releases and EGM2008 up to degree/order 200, evaluated in the white rectangle areas marked in Fig. 8. As a reference, also the standard deviation of the signal is provided

$\sigma_{\Delta g}$[mGal]	North America	South America
Signal	19.15	42.88
TIM_R1	2.59	10.33
TIM_R2	1.67	10.09
TIM_R3	1.41	10.06
TIM_R4	1.21	10.02

the subregion marked by white rectangles in Fig. 8, for all four TIM releases. In North America, where the EGM2008 is expected to have very good quality due to the availability of high-quality ground gravity data, the differences to the GOCE models are generally small, and the consistency steadily increases with increasing release number. From this, we can conclude that the TIM models are not affected by significant systematic errors.

In contrast, in South America, systematic differences to EGM2008 persist for all GOCE releases. In this region, no or only low-accuracy terrestrial gravity field

information exists, resulting in large errors also in the global EGM2008 model. Such significant differences appear also in other regions of the world, such as central Africa, the Himalaya region, or Antarctica. In these regions, due to GOCE, high-resolution gravity field information is available for the very first time, and it is expected that there will be high impact for the geophysical modeling of the lithosphere, e.g., in the active continental margin of the Andes region or the East African rift zone.

Another strategy of external validation is the comparison with independent "direct geoid observations" derived from long-term GPS observations (delivering ellipsoidal heights h) and spirit leveling (providing orthometric heights H), because their difference is the geoid: $N = H - h$. According to the methodology described in Gruber et al. (2011), the models were truncated at a certain maximum degree and order n and filled up beyond with the combined gravity field model EGM2008 (Pavlis et al. 2012) in order to reduce omission errors. Exemplarily, Fig. 9a shows the results for Germany, evaluated at 675 GPS/leveling stations, and Fig. 9b for Japan (873 stations).

In Germany, where the best GPS/leveling data set worldwide is available, the standard deviation between TIM_R4 and the GPS/leveling observations amounts to about 4.5 cm at $n = 200$. Taking into consideration that the GPS/leveling observations themselves are assumed to have errors in the order of 2–3 cm, this number is very consistent with the 3.2 cm "formal" error resulting from the covariance propagation (cf. Table 1). From the results in Japan, we can conclude that the pure GOCE models TIM_R3 and TIM_R4 perform significantly better than EGM2008, even though the latter contains also terrestrial gravity data.
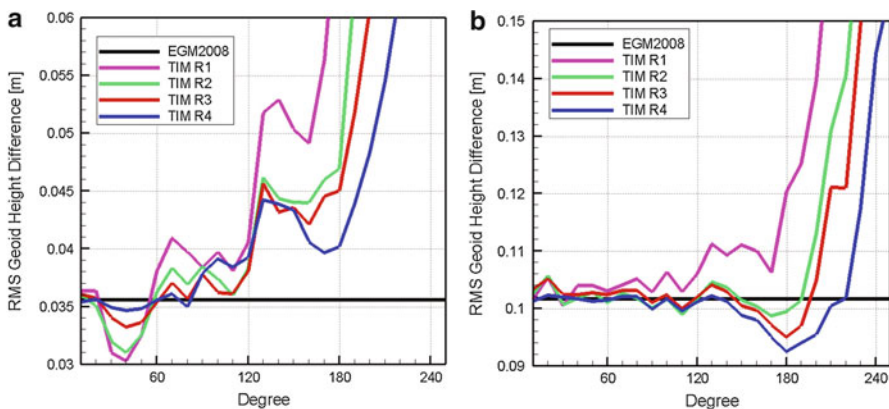

Fig. 9 Standard deviation of geoid height differences σ_N [cm] between gravity field models and GPS/leveling observations in selected regions: (**a**) Germany (675 points); Japan (873 points), truncated at degree/order n

5 Current and Future Perspectives

5.1 Combined Gravity Field Models

In the frame of the project initiative GOCO ("Gravity Observation Combination"; www.goco.eu), consistent combination models from GOCE and complementary gravity field information are computed. With the global gravity model GOCO01S (Pail et al. 2010b), the first combination solution from GRACE (based on ITG-Grace2010S; Mayer-Gürr et al. 2010) and GOCE was computed. Meanwhile, the successor model GOCO03S is available (Mayer-Gürr et al. 2012), which is based on TIM_R3 NEQs, consistently combined with NEQs from GRACE (ITG-Grace2010S), 8 years of CHAMP data, and 5 years of satellite laser ranging (SLR) data to 5 satellites.

Figure 10 shows the formal errors of the model GOCO03S (blue) as well as its two main contributors TIM_R3 (red) and ITG-Grace2010S (green). Due to its measurement technology of low-low SST based on K-band microwave ranging, GRACE is superior in the low to medium degrees of the harmonic spectrum, while GOCE dominates in the higher degrees and thus provides the increased spatial resolution. In this way, the main strengths of these two mission concepts are combined in an optimum way. Also here, the correct stochastic modeling of the individual components and their correct relative weighting is a prerequisite for an optimum combination, especially in the overlapping band of the spectrum where both missions can contribute significantly. Therefore, also in the course of the computation of these combined solutions, the whole arsenal of geomathematical and statistical methods as discussed in Sect. 3 find their application.
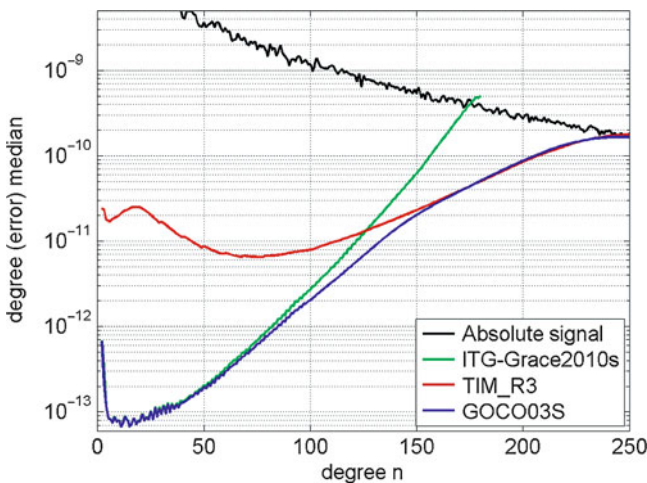

Fig. 10 Degree error medians of GOCO03S and its two main contributors

In addition to these pure satellite-only models, currently also combination models including terrestrial gravity field information on the continents and gravity anomalies derived from satellite altimetry over the oceans are in preparation. Recently, the combined gravity field model TUM2013C, which is based on full NEQs complete to degree/order 720 corresponding to approximately 520,000 unknown gravity field coefficients, has been computed (Fecher et al. 2013). The rigorous solution of these NEQs requires a working memory of more than 2 TB (Fecher et al. 2011) and is performed on a supercomputer at the Leibniz Rechenzentrum (LRZ) in Munich.

5.2   Improved Level 1b Processing

A further gain in performance of GOCE gravity field models could be achieved by an improved method for gravity gradient preprocessing in the frame of the Level 0 to Level 1b processing hosted at ESA. The main impact results from an alternative method for attitude reconstruction from star tracker and gradiometer information based on a Wiener filter (Stummer et al. 2011) and thus an improved separation of linear and angular accelerations. The modifications of the Level 1b processor are described in Stummer et al. (2012). Meanwhile, they have been implemented, and the GOCE data of the full mission period have been reprocessed.

The right column of Fig. 3 shows the significant reduction of long-wavelength errors in the new gravity gradient data. While in the original data the observations were dominated by noise, and therefore features of the gravity field were blurred, in the reprocessed gravity gradients, the signal clearly dominates. The noise reduction mainly in the low frequencies can also be observed in the PSDs shown in Fig. 4.

The impact of this improved gravity gradient performance on gravity field solutions has been assessed by Pail et al. (2013). It could be shown that not only GOCE gravity field models will benefit, but also the accuracy of combined GOCE-GRACE models will improve by up to 15 % also in the higher degrees, which is mainly due to a generally improved performance of the V_{YY} component also within the MBW and, as a result, improved estimates of the sectorial and near-sectorial coefficients up to high degrees. Meanwhile, these reprocessed GOCE gravity gradients have been used to compute the TIM_R4 model (cf. Table 1 and the discussion of results in Sect. 4).

5.3   GOCE Orbit Lowering

By the end of 2012, there was still fuel left on board of the GOCE satellite for about one further year of operation. Additionally, over the whole mission lifetime, the solar activity, and thus also the air drag, has been significantly lower than originally predicted. Therefore, it was decided to lower the satellite's orbit from the original 255 km by about 30 km, in order to counteract signal attenuation with altitude and thus to increase the spatial resolution of the derived gravity field models. This orbit lowering has meanwhile been performed in four steps. The satellite altitude was
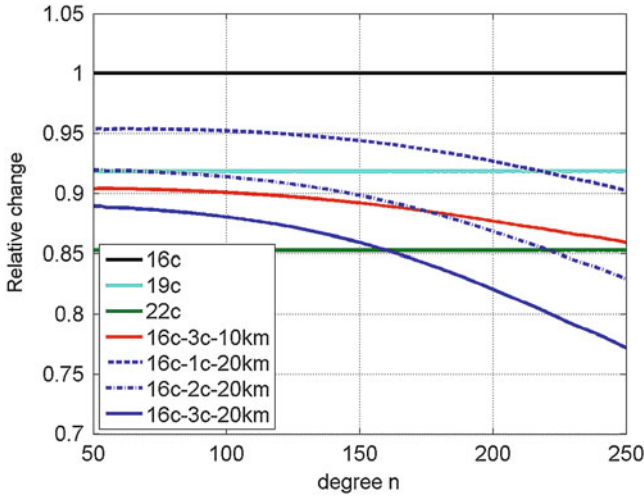
Fig. 11 Performance prediction of last GOCE phase: relative improvement of gravity field accuracy per degree due to orbit lowering

decreased by about 8.6 km in August 2012, by further 7 km in November 2012 and 5 km in February 2013, and GOCE reached its −30 km final altitude of about 225 km in May 2013. GOCE is expected to stay operational at this extremely low altitude until October 2013.

Figure 11 shows a prediction of the impact of lowering the orbit on the achievable gravity field performance. The baseline is represented by the black curve, indicating the performance at the end of the nominal extended mission phase, where full 16 cycles (of about 2 months each) have been completed. A continuation of the mission at the same height for 3 (light blue) or 6 (green) further cycles at 255 km leads to further improvements due to more and more data according to the $\sqrt{N}$ rule, which is constant for all harmonic degrees n. Lowering the satellite by 10 km and flying at 245 km for 3 cycles (red) improves the performance over the whole spectral range compared to the corresponding configuration at 255 km (light blue), but is worse than remaining at the original altitude with the potential to stay there for 6 cycles. However, due to the orbit lowering, the high degrees gain more than the low degrees, which is related to the upward continuation term $(r/R)^{n+1}$ in Eq. (1).

The blue curves show the relative improvements when lowering the satellite by 20 km and then flying 1 cycle (dashed), 2 cycles (dash-dotted), or 3 cycles (solid) at this low altitude of 235 km. Evidently, compared to a 6-month mission extension at 255 km (light blue), which would gain about 8 % in performance, due to the orbit lowering by 20 km, the gravity field performance can be improved by 22 % at degree/order 250.

Weighting gains and risks of such an orbit lowering, the huge potential to improve the estimates of the high-degree coefficients and thus to increase the spatial resolution of the GOCE gravity field models was the decisive factor for the final decision to lower the satellite's orbit in its final phase.

6   Summary and Conclusions

Global gravity modeling from GOCE satellite data requires the application of an arsenal of geomathematical and statistical tools. To fulfill the objective to compute pure GOCE models, which are independent of any other external gravity field information, sophisticated tailored methods have been developed, implemented, and operationally applied to compute, up to now, four releases of TIM gravity field models.

The achievable accuracy increases with the inclusion of more and more GOCE data, following the Gaussian $\sqrt{N}$ rule, and no significant systematics appear. Due to a realistic stochastic modeling of all observation components, which is the key to produce high-quality gravity field solutions, the accompanying (formal) error information in terms of full variance-covariance matrices describes the true errors of the solutions very well. This could be proven by various external validation studies. Consequently, with the latest release of GOCE models, the a priori defined main mission goals could have been largely achieved.

GOCE gravity field models are applied in many geo-scientific disciplines, such as geodesy, oceanography, and solid Earth geophysics. They are used for the global unification of height systems, enabling for the very first time the height transfer over the oceans with reasonable precision. In combination with satellite altimetry, mesoscale geodetic mean dynamic topography (MDT) estimates and geostrophic velocities of global ocean currents down to 80 km can be directly observed from space (Bingham et al. 2011; Knudsen et al. 2011). In this sense, not only the time-variable gravity as it is measured by GRACE (e.g., Kusche 2010) but also the static gravity field as provided by GOCE contributes significantly to an improved understanding of dynamic processes in system Earth.

GOCE gravity field models are also used to constrain density models of lithospheric structures, e.g., in active continental margin areas (Hosse et al. 2011). The use of GOCE models will also further improve the opportunity to formulate models of the crust and to distinguish tectonic lineaments, e.g., in Central-North Africa (Braitenberg et al. 2012).

The consistent combination of GOCE with complementary gravity field information results in further improvements in the long-wavelength range (by GRACE and SLR), and the spatial resolution of satellite-only models can be improved by combination with terrestrial gravity and satellite altimetry data. Technically, this leads to very large normal equation systems, which shall be solved rigorously.

Further improvements of the spatial resolution can be expected from the GOCE satellite's orbit lowering by 20 km in its final phase. This data, observed in a rougher environment, might pose additional challenges to geomathematical and statistic processing tools to achieve optimum global GOCE gravity field models.

References

Badura T (2006) Gravity field analysis from satellite orbit information applying the energy integral approach. Dissertation, 109pp, Graz University of Technology

Bingham RJ, Knudsen P, Andersen O, Pail R (2011) An initial estimate of the North Atlantic steady-state geostrophic circulation from GOCE. Geophys Res Lett 38:EID L01606. American Geophysical Union. doi:10.1029/2010GL045633

Bock H, Jäggi A, Meyer U, Visser P, van den IJssel J, van Helleputte T, Heinze M, Hugentobler U (2011) GPS-derived orbits for the GOCE satellite. J Geod 85(11):807–818. doi:10.1007/s00190-011-0484-9

Braitenberg C, Pivetta T, Li Y (2012) The youngest generation GOCE products in unraveling the mysteries of the crust of North-Central Africa. Geophys Res Abs 14:EGU2012-6022. EGU General Assembly 2012, Vienna

Bruinsma SL, Marty JC, Balmino G, Biancale R, Förste C, Abrikosov O, Neumayer H (2010) GOCE Gravity field recovery by means of the direct numerical method. In: Lacoste-Francis H (ed) Proceedings of the ESA living planet symposium, ESA Publication SP-686, ESA/ESTEC, Noordwijk

EGG-C (2010) GOCE Level 2 Product Data Handbook. GO-MA-HPF-GS-0110, Issue 4.2. European Space Agency, Noordwijk. http://earth.esa.int/pub/ESA_DOC/GOCE/GO-MA-HPF-GS-0110_4.2-ProductDataHandbook_24062010.pdf

Fecher T, Pail R, Gruber T (2011) Global gravity field determination by combining GOCE and complementary data. In: Ouwehand L (ed) Proceedings of the 4th international GOCE user workshop, ESA Publication SP-696, ESA/ESTEC, Noordwijk

Fecher T, Pail R, Gruber T (2013) Global gravity field modeling based on GOCE and complementary gravity data. Int J Appl Earth Observ Geoinf. ISSN (online) 0303–2434. doi:10.1016/j.jag.2013.10.005

Floberghagen R, Fehringer M, Lamarre D, Muzi D, Frommknecht B, Steiger C, Piñeiro J, da Costa A (2011) Mission design, operation and exploitation of the gravity field and steady-state ocean circulation explorer mission. J Geod 85(11):749–758. doi:10.1007/s00190-011-0498-3

Freeden W, Schreiner M (2010) Satellite gravity gradiometry (SGG): from scalar to tensorial solution. In: Freeden W, Nashed MZ, Sonar T (eds) Handbook of geomathematics, vol 2. Springer, Berlin/Heidelberg, pp 269–302

Goiginger H, Pail R (2007) Investigation of velocities derived from satellite positions in the framework of the energy integral approach. In: Fletcher K et al (eds) Proceedings 3rd international GOCE user workshop, ESA SP-627, pp 319–324, ESA, ISBN (Print) 92-9092-938-3. ISSN 1609-042X

Goiginger H, Pail R (2010) Covariance propagation of latitude-dependent orbit errors within the energy integral approach. In: Mertikas SP et al (eds) Gravity, geoid and earth observation, IAG symposia, Chania, vol 135. Springer, pp 155–161. doi:10.1007/978-3-642-10634-7_21

Grafarend EW, Klapp M, Martinec Z (2010) Spacetime modelling of the Earth's gravity field by ellipsoidal harmonics. In: Freeden W, Nashed MZ, Sonar T (eds) Handbook of geomathematics, vol 2. Springer, Berlin/Heidelberg, pp 159–252

Gruber T, Visser PNAM, Ackermann C, Hosse M (2011) Validation of GOCE gravity fieldmodels by means of orbit residuals and geoid comparisons. J Geod 85(11):845–860. Springer. doi:10.1007/s00190-011-0486-7

Hosse M, Pail R, Horwath M, Mahatsente R, Götze H, Jahr T, Jentzsch M, Gutknecht BD, Köther N, Lücke O, Sharma R, Zeumann S (2011) Integrated modeling of satellite gravity data of active plate margins – bridging the gap between geodesy and geophysics. Poster presented at AGU Fall Meeting 2011, San Francisco, 8 Oct 2011

Kargoll B (2007) On the theory and application of model misspecification tests in geodesy. Dissertation, University of Bonn. www.igg.uni-bonn.de/tg/uploads/tx_ikgpublication/Diss_Kargoll.pdf

Kern M, Preimesberger T, Allesch M, Pail R, Bouman J, Koop R (2005) Outlier detection algorithms and their performance in GOCE gravity field processing. J Geod 78(9):509–519. Springer. doi:10.1007/s00190-004-0419-9

Klees R, Ditmar P, Broersen P (2003) How to handle colored observation noise in large least-squares problems. J Geod 76(11–12):629–640. Springer. doi:10.1007/s00190-002-0291-4

Knudsen P, Bingham R, Andersen O, Rio M-H (2011) A global mean dynamic topography and ocean circulation estimation using a preliminary GOCE gravity model. J Geod 85(11):861–879. doi:10.1007/s00190-011-0485-8

Koch KH, Kusche J (2002) Regularization of geopotential determination from satellite data by variance components. J Geod 76:259–268. Springer. doi:10.1007/s00190-002-0245-x

Krasbutter I, Brockmann JM, Kargoll B, Schuh W-D, Goiginger H, Pail R (2011) Refinement of the stochastic model of GOCE scientific data in a long time series. In: Ouwehand L (ed) Proceedings 4th international GOCE user workshop, ESA publication SP-696, ESA/ESTEC, Noordwijk

Kusche J (2010) Time-variable gravity field and global deformation of the Earth. In: Freeden W, Nashed MZ, Sonar T (eds) Handbook of geomathematics, vol 2. Springer, Berlin/Heidelberg, pp 253–268

Lackner B (2006) Datainspection and hypothesis tests of very long time series applied to GOCE satellite gravity gradiometry data. Dissertation, Graz University of Technology, Graz, 187pp

Mayer-Gürr T, Eicker A, Kurtenbach E, Ilk K-H (2010) ITG-GRACE: global static and temporal gravity field models from GRACE data. In: Flechtner F, Gruber T, Güntner A, Mandea M, Rothacher M, Schöne T, Wickert J (eds) System Earth via geodetic-geophysical space techniques, pp 159–168. doi:10.1007/978-3-642-10228-8_13

Mayer-Gürr T, Rieser D, Höck E, Brockmann JM, Schuh W-D, Krasbutter I, Kusche J, Maier A, Krauss S, Hausleitner W, Baur O, Jäggi A, Meyer U, Prange L, Pail R, Fecher T, Gruber T (2012) The new combined satellite only model GOCO03S. In: Presentation at international symposium on gravity, Geoid and height systems GGHS, Venice, 10 Oct 2012

Metzler B, Pail R (2005) GOCE data processing: the spherical cap regularization approach. Stud Geophys Geod 49:441–462. doi:10.1007/s11200-005-0021-5

Migliaccio F, Reguzzoni M, Sansò F, Tscherning CC, Veicherts M (2010) GOCE data analysis: the space-wise approach and the first space-wise gravity field model. In: Lacoste-Francis H (ed) Proceedings of the ESA living planet symposium, ESA Publication SP-686, ESA/ESTEC, Noordwijk

Moritz H (1978) Least-squares collocation. Rev Geophys Space Phys 16(3):421–430

Pail R (2005) A parametric study on the impact of satellite attitude errors on GOCE gravity field recovery. J Geod 79:231–241. Springer. doi:10.1007/s00190-005-0464-z

Pail R, Plank G (2002) Assessment of three numerical solution strategies for gravity field recovery from GOCE satellite gravity gradiometry implemented on a parallel platform. J Geod 76:462–474. Springer. doi:10.1007/s00190-002-0277-2

Pail R, Goiginger H, Mayrhofer R, Schuh W-D, Brockmann JM, Krasbutter I, Höck E, Fecher T (2010a) Global gravity field model derived from orbit and gradiometry data applying the time-wise method. In: Lacoste-Francis H (ed) Proceedings of the ESA living planet symposium, ESA Publication SP-686, ESA/ESTEC, Noordwijk

Pail R, Goiginger H, Schuh W-D, Höck E, Brockmann JM, Fecher T, Gruber T, Mayer-Gürr T, Kusche J, Jäggi A, Rieser D (2010b) Combined satellite gravity field model GOCO01S derived from GOCE and GRACE. Geophys Res Lett 37:EID L20314. American Geophysical Union. doi:10.1029/2010GL044906

Pail R, Bruinsma S, Migliaccio F., Förste C, Goiginger H, Schuh W-D, Höck E, Reguzzoni M, Brockmann JM, Abrikosov O, Veicherts M, Fecher T, Mayrhofer R, Krasbutter I, Sansó F, Tscherning CC (2011) First GOCE gravity field models derived by three different approaches. J Geod 85(11):819–843. Springer. doi:10.1007/s00190-011-0467-x

Pail R, Fecher T, Murböck M, Rexer M, Stetter M, Gruber T, Stummer C (2013) Impact of GOCE level 1b data reprocessing on GOCE-only and combined gravity field models.

Studia geophys geod. 57, pp 155–173. doi:10.1007/s11200-012-1149-8, Available online: www.springerlink.com/openurl.asp?genre=article&id=doi:10.1007/s11200-012-1149-8

Pavlis NK, Holmes SA, Kenyon SC, Factor JK (2012) The development and evaluation of the Earth gravitational model 2008 (EGM2008). J Geophys Res 117(B04406):38. doi:10.1029/2011JB008916

Rummel R (2010) GOCE: gravitational gradiometry in a satellite. In: Freeden W, Nashed MZ, Sonar T (eds) Handbook of geomathematics, vol 2. Springer, pp 93–103. ISBN (Print):978-3-642-01545-8, ISBN (Online):978-3-642-01546-5, doi:10.1007/978-3-642-01546-5_4

Rummel R, Gruber T, Koop R (2004) High level processing facility for GOCE: products and processing strategy. In: Lacoste H (ed) Proceedings 2nd international GOCE user workshop "GOCE, The Geoid and Oceanography", ESA SP-569, ESA, Noordwijk

Rummel R, Yi W, Stummer C (2011) GOCE gravitational gradiometry. J Geod 85(11):777–790. Springer. doi:10.1007/s00190-011-0500-0

Schuh W-D (1996) Tailored numerical solution strategies for the global determination of the Earth's gravity field. Mitteil Geod Inst TU Graz 81:156

Siemes C (2008) Digital filtering algorithms for decorrelation within large least squares problems. Dissertation, University of Bonn

Sneeuw N, van Gelderen M (1997) The polar gap. In: Geodetic boundary value problems in view of the one centimeter geoid. Lecture notes in Earth sciences, vol 65. Springer, Berlin, pp 559–568. doi:10.1007/BFb0011699

Stetter M (2012) Stochastische Modellierung von GOCE-Gradiometerbeobachtungen mittels digitaler Filter. Master's Thesis, no. D240, TU München

Stummer C, Fecher T, Pail R (2011) Alternative method for angular rate determination within the GOCE gradiometer processing. J Geod 85(9):585–596. Springer. doi:10.1007/s00190-011-0461-3

Stummer C, Siemes C, Pail R, Frommknecht B, Floberghagen R (2012) Upgrade of the GOCE level 1b gradiometer processor. Adv Space Res 49(4):739–752. doi:10.1016/j.asr.2011.11.027